

Thesis Draft

Andreas Ramsli

March 6, 2023

Contents

1	Introduction	2
2	Theory	2
2.1	GRB observations	2
2.1.1	GRB classifications	2
2.1.2	Describing a GRB spectrum	2
2.2	xspec	3
2.2.1	Spectrums	3
2.2.2	Response files	3
2.2.3	Fitting procedure	3
2.2.4	Optimalization	4
3	Instruments and datasets	5
3.1	General Overview of Instrumentation	5
3.2	ASIM	5
3.2.1	HED Safety Time Criteria	5
3.3	Konus-Wind	5
3.4	FERMI	6
4	Methods	6
4.1	GRB identification in ASIM	6
4.2	ASIM data preparation	6
4.2.1	Harvesting ASIM data	6
4.2.2	Absolute timing correction	6
4.2.3	Energy calibration	6
4.2.4	Safety Time	7
4.2.5	Cross Correlation of Light Curves	7
4.2.6	FITS files	8
4.3	Spectral fitting	8
4.4	ASIM data consistency check	8
4.4.1	Light Curve Analysis	9
4.4.2	Background ratemeter analysis	9
4.4.3	DRM analysis	10
4.4.4	MXGS Polar Coordinate	11
4.4.5	Statistics on the calibration coefficients	13
5	Results and discussions	14
5.1	ASIM GRB database	14
5.1.1	GRB detections	14
5.1.2	GRB data availability	15
5.1.3	GRB spectral intervals and ToF	16
5.1.4	Model parameters	17
5.1.5	KW model parameters	17
5.1.6	Normalization constant	18
5.1.7	Correlation between KW-ASIM and KW spectral analysis	18

5.1.8	Calibration Coefficients for KW-ASIM-FERMI and KW-ASIM Spectral Analysis . .	19
5.2	Case studies	20
5.2.1	GRB 210619B	20
5.2.2	GRB 211211A	20
5.3	GRB classifications	20
5.4	ASIM performance assessment and outlook	20
6	Summary and outlook	20
7	Appendix I: GRB Archive	20
8	Appendix II: ASIM Fits Software	20
9	Appendix III: Code & Data	20
10	Abbreviations	20

1 Introduction

2 Theory

1. GRB observations
 - General introduction to GRB. Classification (short / long), distribution, production mechanism, measured redshift (distance)
2. General info and overview of the data. The details go into the methods chapter
3. xspec spectrums

2.1 GRB observations

Gamma-ray bursts (GRBs) are some of the most powerful events in the universe, releasing an enormous amount of energy in mere seconds. They can be categorized into two main groups based on their progenitor: binary compact object mergers and collapsars. Binary compact object mergers involve the coalescence of two compact objects such as neutron stars or a neutron star and a black hole, and they produce short GRBs (≤ 2 s). On the other hand, collapsars result from the collapse of massive stars to a compact object and produce long GRBs (> 2 s). Additionally, the pulses in short GRBs exhibit exponential rises and fast decays (ERFD) in contrast to the fast rise exponential decay (FRED) pulses of long GRBs. Furthermore, long-duration GRBs have a softer spectrum compared to short-duration GRBs.

In order to validate the performance of ASIM, it is crucial to compare its spectrum to that of other instruments. In this report, we present a cross-calibration of the energy response of ASIM, KW, and FERMI by analyzing GRBs that were observed simultaneously. These GRBs serve as standard candles and enable us to validate the response of ASIM in comparison to other instruments. By using this approach, we can effectively evaluate the accuracy and reliability of ASIM's measurements and energy response.

2.1.1 GRB classifications

Provide more information about the classification found in Zhang book.

2.1.2 Describing a GRB spectrum

The average energy of a gamma-ray photon can vary greatly depending on the source of the gamma rays. For example, gamma rays emitted by the sun have an average energy of about 1 keV, while gamma rays emitted by a GRB can have an average energy of about 1 MeV.

GRBs emit non-thermal radiation, which is characterized by a power-law distribution of flux that extends to higher energies than thermal radiation. This requires that electrons be accelerated in non-equilibrium environments such as shocks or magnetic reconnection sites. To extract the GRBs' spectra, the accumulation of photons over a certain interval of time is necessary. Due to the highly variable nature of GRBs, ideally one should extract spectra in small time bins to study the evolution of spectral properties. The read-out electronics for MXGS allows for a high resolution of the detected photons. There are four ways to display GRBs spectra: raw photon count (in units of $cts \cdot s^{-1} \cdot keV^{-1}$), photon number ($photons \cdot cm^{-2} \cdot s^{-1} \cdot keV^{-1}$), specific flux density ($erg \cdot cm^{-2} \cdot s^{-1} \cdot keV^{-1}$), and energy spectrum ($erg \cdot cm^{-2} \cdot s^{-1}$).



2.2 xspec



When studying the spectrum of a source, it is important to consider the specific characteristics of the instrument used to make the measurement. `xspec`, a popular software tool used for analyzing gamma-ray data, requires knowledge of the instrument's response and background to produce accurate results.

2.2.1 Spectrums

When analyzing the spectrum of a source, there are different ways to describe the distribution of radiation in energy. The raw photon count spectrum $C(E)$ shows the detected photon counts as a function of energy bin, but is heavily affected by the detector's instrumental response function. The photon number spectrum $N(E)$, in units of $photons \cdot cm^{-2} \cdot s^{-1} \cdot keV^{-1}$, corrects for instrumental response function effects and is the most straightforward spectrum to obtain. The peak in the spectrum corresponds to the energy at which the source emits the most radiation.

Another way to display the spectrum is through a spectral energy distribution (SED), which shows the source's energy distribution in frequency or energy. The SED is typically expressed as νF_ν or $E^2 N(E)$, often in units of $keV^2 (photons \cdot cm^{-2} \cdot s^{-1} \cdot keV)$. This type of spectrum is of theoretical interest and can provide valuable information about the properties of the source.



2.2.2 Response files



The response of an instrument is proportional to the probability that an incoming photon of energy E will be detected in channel I . As such, the response is a continuous function of E , which is converted to a discrete function through the use of a response matrix. The response matrix defines the energy ranges E_j and the response $R_D(I; J)$ for each channel, with `xspec` reading both the energy ranges and the response matrix from a response file in a compressed format that only stores non-zero elements.

The response matrix is defined as:

$$R_D(I, J) = \frac{\int_{E_{j-1}}^{E_j} R(I, E) dE}{E_j - E_{j-1}} \quad (1)$$

where $R_D(I, J)$ is the response for channel I and energy range J , and $R(I, E)$ is the instrumental response function for energy E and channel I .

`xspec` also includes an option to use an auxiliary response file, which contains an array $A_D(J)$ that is multiplied into $R_D(I; J)$. This array represents the efficiency of the detector, with the response file representing a normalized Redistribution Matrix Function, or RMF. Conventionally, the response is in units of cm^2 . The auxiliary response file is particularly useful for correcting for the effects of dead time and pile-up, which can significantly impact the accuracy of the measured spectrum. By including information about the detector's efficiency and the RMF, `XSPEC` is able to accurately model the measured spectrum and obtain more reliable parameter values for the physical properties of the source.

2.2.3 Fitting procedure

In order to obtain the actual spectrum of a source, `xspec` uses a "best-fit" model that can be described in terms of a few parameters. For each model spectrum $f(E)$, a predicted count spectrum $C_p(I)$ is calculated and compared to the observed data $C(I)$. A "fit statistic" is computed from the comparison

and used to judge whether the model spectrum “fits” the data obtained by the spectrometer. The model parameters are then varied to find the parameter values that give the most desirable fit statistic, and these values are referred to as the best-fit parameters. The model spectrum, $f_b(E)$, made up of the best-fit parameters is considered to be the best-fit model.

After obtaining a best-fit model, `xspec` can also determine the confidence intervals of the best-fit parameters. The confidence intervals can be calculated using the “error” command, which calculates the error on a particular parameter by varying it until the fit statistic increases by a certain amount above the best-fit value. The error command takes as arguments the parameter to examine and the delta fit statistic, $\Delta\chi^2$, which is a real value that indicates the delta fit statistic, as well as the other non-frozen parameters.

When fitting data to a model using XSPEC, the chi-squared test is a commonly used statistic to compare the observed data to the model. This statistic is sensitive to the number of counts in each bin, so we use the command `grppha` to group the energy bins to have a minimum of 20 counts in each. The sum of the squared differences between the observed data and the model is used as a measure of the goodness of fit. Additionally, the confidence range for a parameter in a model is determined by the uncertainties in the parameter’s value based on the statistical analysis of the data. This range can be asymmetric, meaning the upper and lower limits are not equally distant from the central value. While the confidence range reflects the range of values that are most consistent with the data given a certain level of confidence (such as 68% or 90%), it’s important to note that it’s not the same as the possible range of values for a parameter. The level of certainty about the true value of the parameter given the data we have can cause the upper limit of the confidence range to be more positive than the lower limit, or vice versa. As the confidence level increases, the likelihood of the true value of the parameter lying outside of the confidence range decreases.

The normalization parameter is another essential parameter in fitting models to data. It provides an overall scaling factor for the model, allowing you to compare the model spectrum to the observed data. The normalization parameter is typically given in units of photons or energy per unit area per unit time per unit energy (e.g., $\text{ph cm}^{-2} \text{s}^{-1} \text{keV}^{-1}$). The best-fit normalization value can provide information about the intrinsic luminosity of the source and estimate the total number of photons emitted by the source at a particular energy range. Additionally, the normalization can be used to compare different observations of the same source or different sources, providing a way to normalize the spectra and compare their shapes and slopes.

2.2.4 Optimization

The error command explores the parameter space in the neighborhood of the best-fit values and may find better minima with lower $\Delta\chi^2$ values. By default, the initial value for the delta fit statistic is 2.706, which is equivalent to the 90% confidence region for a single interesting parameter. Note that before the error command is executed, the data must be fitted.

If the error command is not well behaved and it outputs a warning about a “non-monotonicity in statistic space detected”, it might be that the algorithm have gotten stuck in a local minima. To resolve this issue it’s advised that the `steppar` command is used to approximate a better parameter value. To visualize the χ^2 vs parameter value, use `plot contour`. Intuitively, what we are doing is to test out a range of values for the parameter to achieve a better χ^2 . See example below.

It’s possible to get stuck in a local minimum, even after applying the `steppar` command. If a “new best fit” message appears, it indicates that a better χ^2 value has been found during the procedure, and the parameter in the model will be updated accordingly. However, it’s important to note that a better fit might be achieved without the “new best fit” message being shown. This could be because the new χ^2 value isn’t improved by a certain value. Therefore, to optimize the model, it’s essential to manually verify that the current parameter value is indeed the global minimum by visually inspecting the contour plot and using the `steppar` command to iterate closer to the global minimum. Once the global minimum value has been found, the parameter value can be set to that value using the `newpar` command, and then the `fit` command can be run. This will optimize the model around the global minimum and find the “best fit” model for the spectra.

To summarize, XSPEC combines observed photon count spectra, instrument response functions, and best-fit models to accurately determine the physical properties of astronomical sources. The goodness-

of-fit and confidence interval calculations provide a measure of the accuracy and reliability of the results. By utilizing these techniques, XSPEC provides a powerful tool for fitting the spectra for GRBs.

3 Instruments and datasets

3.1 General Overview of Instrumentation

1. Table showing key instrument information and capabilities
2. Graphical overview; solar system illustration

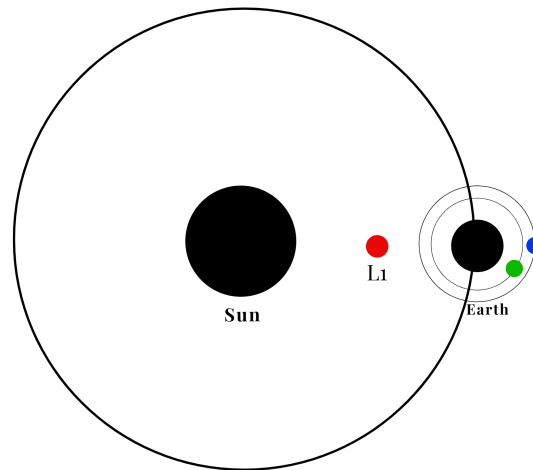


Figure 1: KW is located at L_1 and ASIM and FEMRI is in low Earth orbit



3.2 ASIM

- mission profile and capability as GRB detector
- MXGS; Designed to trigger on short and energetic TGF's. These have generally higher fluxes than GRB's. Hence, when ASIM is detecting GRBs, the MXGS instrument suffers very little instrumental effects, making it an capable GRB detector.
- Illustrations of ASIM mounted on ISS and coordinate plane (theta, phi)
- BGO/CZT DRM plots from David showing effective area
- HED Safety Time Criteria

3.2.1 HED Safety Time Criteria

For high fluxes and high energy photons the HED instrument suffers from high voltage drops in the PMTs which have to be handled carefully [Lindanger et al., 2021].

1. why does HED suffer from high voltage drop and how does that effect the data?
2. plot of the energy vs st and explain how this was constructed
3. how are the counts that meet the ST criteria handled?
4. point out of that the st is different for each BGO and it doesn't affect the other BGOs

3.3 Konus-Wind

- mission profile and the long history of reliable operation. Include info on the trigger logic and spectrum accumulation time. See the Tsvetkova paper for instrumentation info.
- detector area. Explain how the detectors are oriented (top/bottom)

- Energy range of the instrument have been shifting over the years (see Tsvetkova paper)
- The Konus-Wind instrument initial paper (Aptekar et al. 1995)
- been operational since 1994, can provide us with spectral and temporal data about GRBs in the broad-band energy coverage (10-10000 keV)
- spectrums are provided by our research colleagues at Ioffe institute/Sardinia (anastasia ++)

3.4 FERMI

- mission profile and the long history of reliable operation. Include reference to the FERMI database



what is the detector area of each BGO and NaI?

4 Methods

4.1 GRB identification in ASIM

Our objective was to establish a correspondence between the ASIM trigger list and gamma-ray bursts (GRBs) identified by the Interplanetary Network (IPN) or the ICECUBE collaboration. The ASIM trigger list contained approximately 270,000 triggers for both HED and LED in the period from June 1st, 2018, until December 31st, 2021. The majority of these triggers were related to atmospheric phenomena or high-energy particles from the solar wind.

To find a correspondence, we exported a csv file from the IPN catalog, which contains all the identified GRBs detected by KW and FERMI during the previously mentioned time period. However, during the time of exporting the IPN catalog, it did not contain triggers up until the end of 2021. Therefore, we supplemented it with more recent GRBs provided in the ICECUBE catalog.

After the data preparation, we searched for a correspondence between ASIM and the catalogues within a time window of ± 10 seconds, taking into account the propagation time of the photons between the instruments. Our initial search resulted in 31 matches, which required further investigation to verify that they were indeed GRBs. We extracted the ASIM light curve and cross-checked it with the other instruments to eliminate chance coincidences and insignificant signals. Ultimately, we identified 12 promising GRB candidates for spectral analysis.

4.2 ASIM data preparation

To prepare the ASIM data for spectral analysis, we extracted several important metrics from the ASIM database. It should be noted that all of our 12 GRB candidates are triggers in the high-energy detector (HED). To extract the ASIM data for our GRB candidates, a MATLAB code developed by the researchers at UiB was utilized. Once the data was extracted, it was imported into a Python environment for data analysis. The relevant data extracted includes the *tus*, which is the time of arrival of individual photons with microsecond resolution relative to the T0. Each detected photon has a corresponding BGO address (1-12), detector assembly unit address (DAU) (1-4), detector address (DET), energy channel (0-4095), and type (1-3). Handling this large amount of ASIM data required the use of important libraries such as Pandas and NumPy to create a DataFrame or matrix.



~~4.2.1 Harvesting ASIM data~~

~~4.2.2 Absolute timing correction~~

4.2.3 Energy calibration

To ensure accurate energy measurements, we calibrate the energy channel to keV using time-dependent calibration coefficients for each BGO with a quadratic fit. The equation used for the calibration is Energy [keV] = $A \times \text{CHANNEL}^2 + B \times \text{CHANNEL} + C$, where A, B, and C are the calibration coefficients that are determined using the 511 keV line, the 1274.5 keV line, and the proton peak (at about 31 MeV) in the background energy spectrum. For each burst, a specific set of calibration coefficients had to be retrieved and applied. In the following chapters, we will present a statistical investigation into these calibration


coefficients to ensure the accuracy of our spectral analysis. **any references to this energy calibration coefs. by David?**



4.2.4 Safety Time

4.2.5 Cross Correlation of Light Curves

Cross-correlation is a mathematical technique that allows us to measure the similarity between two signals as a function of time lag. In the context of joint spectral analysis, cross-correlating the light curves (LCs) of different instruments is a crucial step in preparing the data. This is because each instrument has a different trigger logic, leading to different reference times (T_0) for each instrument. Cross-correlation is necessary to accurately align the LCs in the correct reference frame and ensure that ~~the data can be calibrated correctly.~~

Our objective with the cross-correlation is to bring the relevant LCs into the correct reference frame, usually that of the KW instrument. The accumulation time of the spectrum is fixed by the KW instrument's trigger logic.  Our research colleagues handling the KW instrument provide us with the LCs for all the GRB candidates that were simultaneously triggered by KW. These LCs have varying bin sizes in powers of 2, starting from 2 ms. Depending on the nature of the burst, we choose the most relevant bin size for our cross-correlation and cut the LC at the appropriate time interval. We initially shift the ASIM and FERMI data based on the instrument's T_0 and the time of flight (ToF) to center the relevant LCs at approximately the same T_0 , facilitating the cross-correlation between the LC objects.

To perform the cross-correlation, we use the software `stingray` [Bachetti et al., 2022] in a Python environment. A LC object is created for each instrument, either from an array of photon arrival times or from a histogram with bin counts and bin edges passed as parameters. The LC objects' bin edges must be identical. Once we have our LC objects, we create a cross-correlation object with the LC objects passed in as parameters. From this cross-correlation object, we can estimate which time lags will produce the highest correlation between the LC objects.

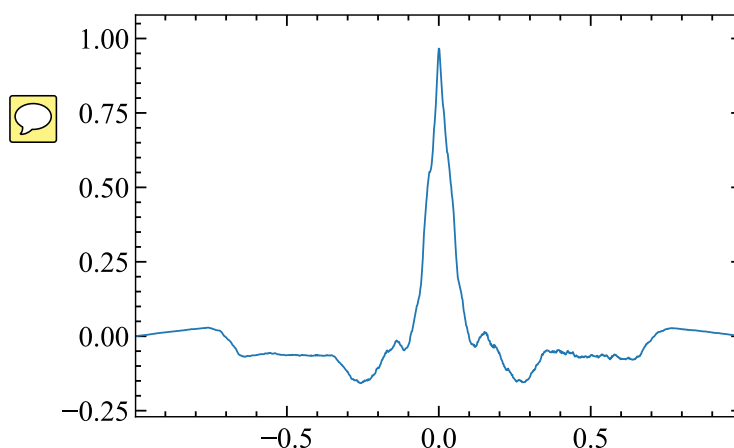




Figure 2: Example CC plot of GRB181222B between KW and ASIM. The x-axis shows the different time lags in seconds and the y-axis shows the normalized correlation.

In figure 2, an example of a cross-correlation plot is shown, displaying the correlation between the ASIM and KW LC object.  The cross-correlation plot is normalized, such that perfect correlation gives 1, and perfect anticorrelation gives -1. From this cross-correlation object, the optimal time lag that produces the highest correlation is given in seconds. Note that the ASIM LC have already been shifted by the optimal time lag.  Once the ASIM and/or FERMI data have been shifted by this time lag, the data are brought into the reference frame of KW. The data are now ready for the next step in data preparation.

4.2.6 FITS files

1. exporting the ASIM data from CDF format (stored in DK server) to FITS format, which is the standard format used for spectral analysis in xspec
2. extracting the spectrums based on time intervals found in 3
3. we cut the ASIM data in that interval and bin the energies in log increasing bins from 10 keV to 100 MeV. (The background interval is also binned in the same energy bins)
4. the rsp file contain the DRM given by the incoming theta, phi angle, more information about the rsp files are found in theory section xspec section
5. Creating pha, bak and rsp files. reference the appendix for more information about the SW developed for this procedure.

4.3 Spectral fitting

In this section, we describe the models used for spectral fitting in our analysis. The joint spectral fits are performed by xspec (ver. 12.13.0c). We use two models for our fits, a cutoff power-law (CPL) model and the Band function.

The CPL model is described by the equation:

$$f(E) = K_{100}^{\text{CPL}} \left(\frac{E}{100 \text{ keV}} \right)^{\alpha^{\text{CPL}}} \exp \left[\frac{-E(2 + \alpha^{\text{CPL}})}{E_{\text{peak}}} \right], \quad (2)$$

where α^{CPL} is the power-law photon index, K_{100}^{CPL} is the normalization at 100 keV in units of photons $\text{cm}^{-2} \text{ keV}^{-1}$, and E_{peak} is the peak energy in the νF_{ν} spectrum.

The Band function is described by the equation:

$$f(E) = \begin{cases} K_1 \left(\frac{E}{100 \text{ keV}} \right)^{\alpha} \exp \left[-\frac{E(2+\alpha)}{E_{\text{peak}}} \right], & E < \left[\frac{(\alpha-\beta)E_{\text{peak}}}{(2+\alpha)} \right] \\ K_1 \left[\frac{(\alpha-\beta)E_{\text{peak}}}{(2+\alpha)100 \text{ keV}} \right]^{\alpha-\beta} \left(\frac{E}{100 \text{ keV}} \right)^{\beta}, & E \geq \left[\frac{(\alpha-\beta)E_{\text{peak}}}{(2+\alpha)} \right] \end{cases} \quad (3)$$

where α is the lower energy photon index, β is the high-energy photon index, E_{peak} is the peak energy in the νF_{ν} spectrum, and K_1 is the normalization at 100 keV in units of photons $\text{cm}^{-2} \text{ s}^{-1} \text{ keV}^{-1}$. The two spectral regimes are separated by the break energy E_0 . The peak energy (E_{peak}) in the νF_{ν} spectrum is related to the break energy (E_0) through:

$$E_{\text{peak}} = (2 + \alpha)E_0 \quad (4)$$

We use the Band function as our primary model for spectral fitting.

We perform our spectral fits using xspec in a Linux and macOS environment. The spectral models described above are used as input for the fitting process. We multiply the model by a constant factor to understand the calibration uncertainties among the instruments. The constant factor for the KW data was fixed to 1, and the constant factors of the ASIM and FERMI instruments are kept as free parameters. The fitting results provide us with estimates for the model parameters and associated errors. These results are used to determine the physical properties of the observed sources and the performance of the instruments compared to KW.

4.4 ASIM data consistency check

The ASIM data consistency check was initiated due to an unexpected deviation in the calibration coefficient for ASIM/HED (C_A) by a relatively large factor, which can be found in table 4. Our analysis required an acceptable calibration coefficient to deviate no more than 20% from unity. However, events such as GRB190206A and GRB190305A had a calibration coefficient of 2.71 and 0.349, respectively. This indicates that the HED detected **times more counts** than KW for 190206A, and 0.349 times less for 190305A. To identify the cause of the problem, we examined various factors **For** example, we investigated the background used in ASIM data.

4.4.1 Light Curve Analysis

In this section, we present our analysis to verify that we are extracting the correct spectrum from the correct interval defined in Table 3 for the selected GRBs with a bad calibration coefficient. Our hypothesis was that we were extracting the burst or background spectrum at the wrong interval. To check this hypothesis, we performed a LC analysis and verified that we were extracting the proper spectrum for our given interval. We observed a calibration coefficient of ~ 0.35 in GRB190305A, indicating that we detected 65% fewer counts than KW during the same time interval. This suggests that the burst spectrum might not have been accumulated at the appropriate time interval. However, the LC analysis for the bursts that have a discrepancy in the calibration coefficient indicates that we were extracting the spectrums at the proper time intervals. Therefore, the cause of the discrepancy in the calibration coefficient must be due to another factor.

4.4.2 Background ratemeter analysis

In this subsection, we investigate whether we can rely on the accumulated background spectra by analyzing the background count rate for the ASIM instrument at the given magnetic latitude (mlat). ASIM experiences high background radiation at high mlat due to cosmic rays. Furthermore, at high mlat, more photons with lower energies can penetrate deeper into the magnetosphere, causing a higher background rate. Conversely, at lower mlat, ASIM experiences a lower background rate because the low-energy photons are absorbed or scattered at higher altitudes in the Earth's magnetosphere. ASIM has a protective mechanism called 'decimation mode,' which is activated when the background rate increases above a certain level. This protective mechanism is necessary because the ISS passes through the Earth's radiation belt, where charged particles are trapped. We conclude that the decimation mode was not activated during any of the background spectrum accumulation times.

We first conducted ratemeter analysis of 15 orbits of the ISS, where we extracted the background count rate, datetime, latitude, longitude, and altitude of ASIM for each sample. We estimated the magnetic latitude (mlat) using the ApexPy library, and used MATLAB to create a scatter plot of the ratemeter versus mlat, and estimated the envelope of the ratemeter data points. We then calculated the background count rate (cts/s) for all of our background files, which were used in the spectral analysis. In some cases, we could use the background found in the same trigger data as the burst, but in other cases, we used another trigger file that was sufficiently close in time to the burst trigger, to accumulate a background. Finally, to show that the background count rate found in the data files used in the analysis were as expected, we plotted them on top of the estimated background envelope.

We estimated the background count rate (cts/s) for each of our background files, which were used in the spectral analysis. For some bursts, we could use the background found in the same trigger data as the burst. However, in other cases, there was not enough time to accumulate a background. This was because trigger data for ASIM is accumulated for a maximum of 2 seconds for each trigger. In such cases, we used another trigger file that was sufficiently close in time to the burst trigger to accumulate a background. This was only the case for a few bursts, and we could use the background data found in the burst trigger file in most cases.

We estimated the envelope of the ratemeter data points using MATLAB. To create the scatter plot of the ratemeter versus mlat, we interpolated using a 5th degree polynomial and applied a sinus function with noise to estimate the upper and lower boundaries of the envelope. We then filled in the area between the upper and lower boundaries to create the envelope. This envelope provides a visual representation of the expected range of background count rates for the given mlat.

To show that the background count rate found in the data files used in the analysis were as expected, we plotted them on top of the estimated background envelope. Figure 3 shows the background count rate from the GRBs within the background envelope. This suggests that the background data files used in the spectral analysis have the expected count rate at the given mlat. This ratemeter analysis has also been performed previously, and the scatter plot of the background count rate as a function of mlat from the previous analysis can be found in figure 4. The background count rate between these two plots is similar.

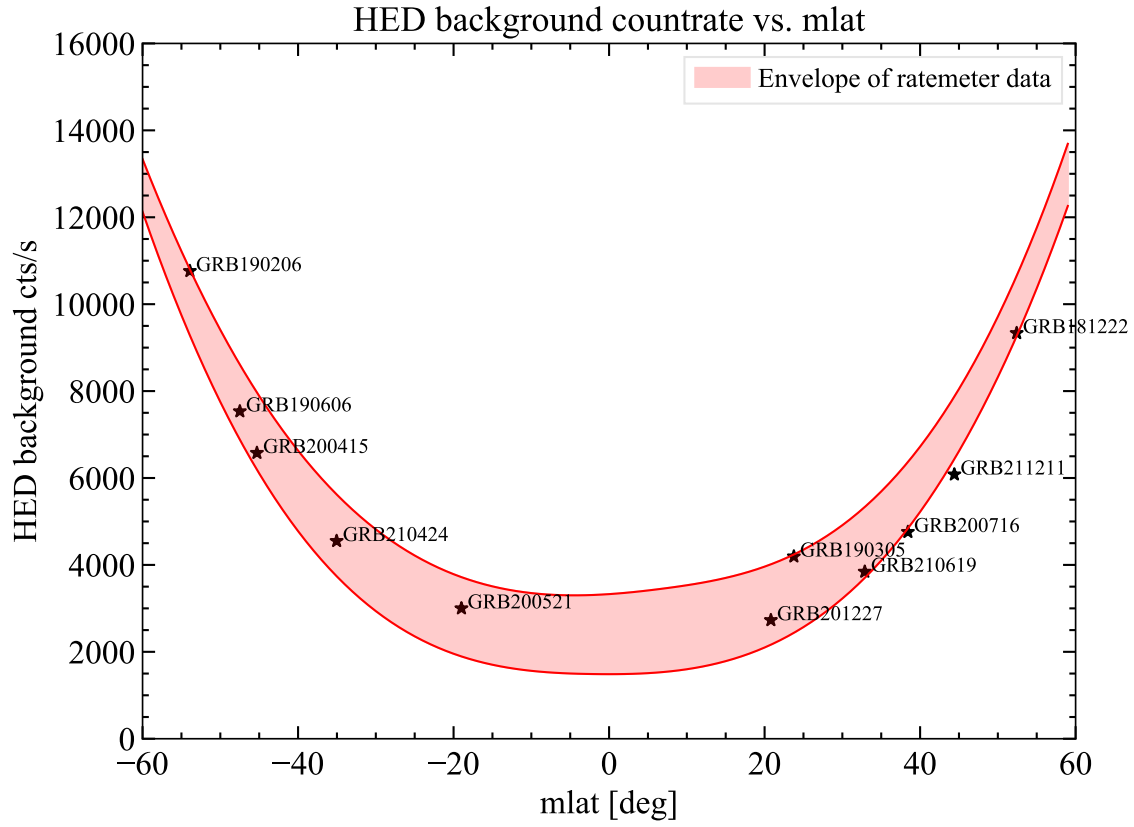


Figure 3: Envelope in shaded red showing the expected count rate for the given magnetic latitude. GRBs shown as stars

4.4.3 DRM analysis



Validation of absorption of radiation by Columbus module for a given theta, phi angle (provide image of coordinate system) and absorption plot.

Responses for $\theta = 90^\circ$ and 105° also analyzed for 0.5 and 1 MeV, but found no discrepancies in the effective area. Observed the expected occultation from the Columbus module at the same φ interval observed in figure 6.

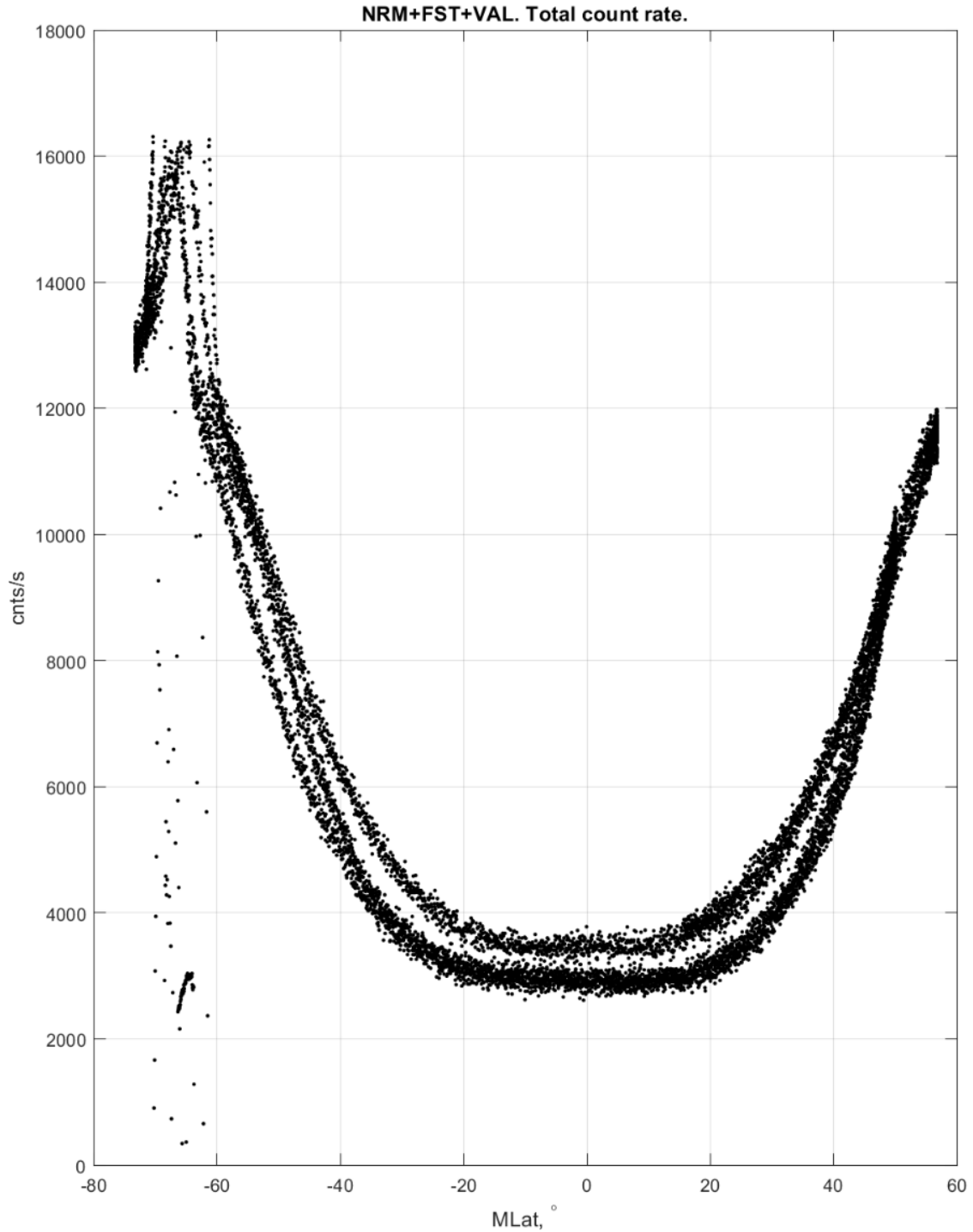


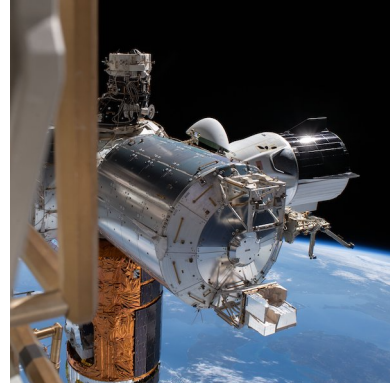
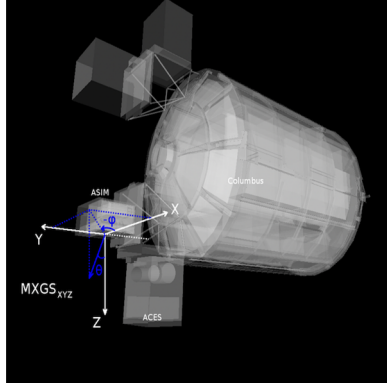
Figure 4: Caption



4.4.4 MXGS Polar Coordinate

The polar plot in Figure 7 displays the incoming ϑ and φ angles of GRBs using scatter points. The color coding in the legend represents the normalization constant, with unity indicated by the specific color. Observing regions that are obscured by the Columbus module or the Earth are represented by shaded areas. **additional info:**

1. What information does the scatter plot convey (occulted sectors, etc.)
2. Particular groupings?



(a) MXGS and ISS coordinate systems are drawn; polar θ and azimuthal ϕ are indicated. Columbus module is located $\phi \approx 90^\circ$, since ϕ is defined as negative in the (b) ASIM mounted on the Columbus module. SpaceX's Dragon docked on the right side

Figure 5: ASIM Mounted on the ISS

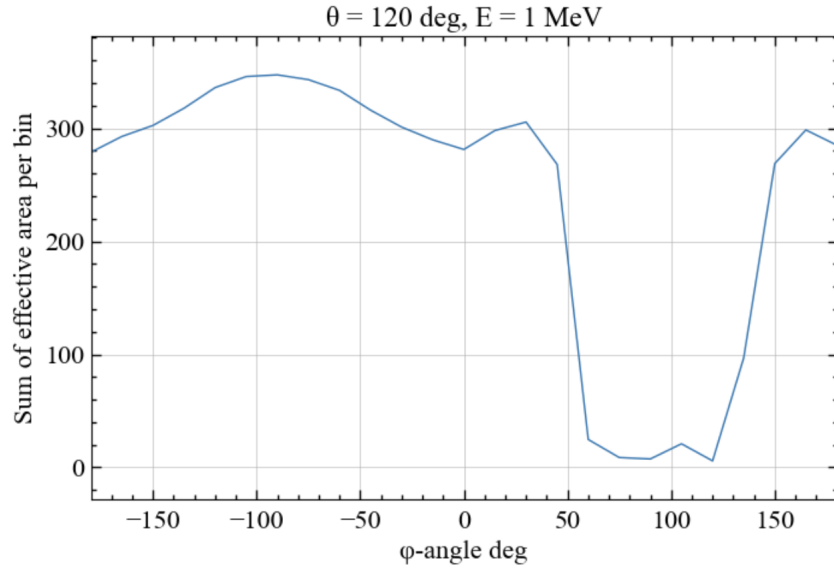


Figure 6: Sum of effective area (cm^2) per bin for HED at $\theta = 120^\circ$ as a function of ϕ . Input energy 1 MeV. Due to the Columbus module, which is located around 45° to 135° the effective area drops almost to zero.

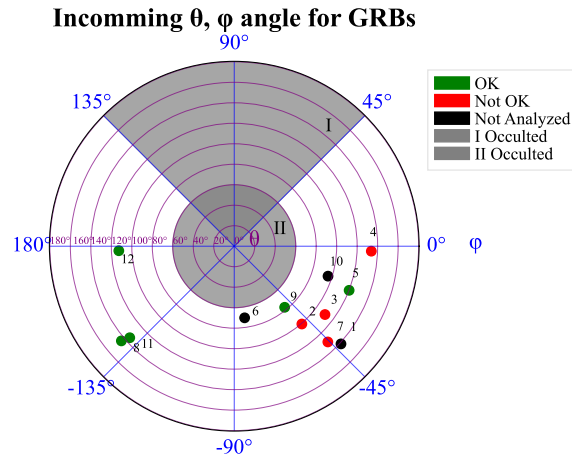


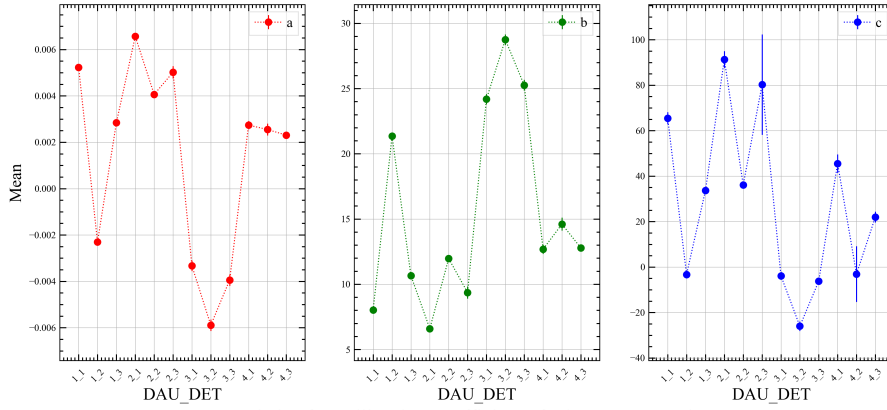
Figure 7: Polar plot of the incoming GRB's θ, ϕ angle. Sector 1 and 2 is occulted respectively by the Columbus module and by Earth. GRB numbering in sorted order from old to new.

4.4.5 Statistics on the calibration coefficients

In our study, we investigated if there were any discrepancies in the calibration coefficients used in our sample. The coefficients a , b , and c are used to convert the energy channel to keV using a quadratic approximation $keV = a \times channel^2 + b \times channel + c$, where the energy channel is between 0 and 4095. The coefficients are generated twice a day, around midnight and midday (UTC), and are known to change slightly over time. We observed that some GRBs in our sample had a normalization constant that deviated by a factor of ~ 2.7 or ~ 0.3 from unity. To analyze the consistency of ASIM data, we extracted the calibration coefficients used in our GRB sample and sampled the coefficients closest in time to our T0. We computed the mean, standard deviation, minimum, and maximum of the coefficients, which were then stored in a large table.

To better understand if there were any underlying discrepancies that evolved over time, we produced scatter plots of the mean as the data points and the standard deviation of the mean as the error bars for each coefficient. The leftmost scatter plot shows the coefficient "c", and we observed that the error on "DAU 2 DET 3" and "DAU 4 DET 2" was large compared to the other data points, indicating that the "c"-value has a wide range in the dataset. In fact, the minimum and maximum values were respectively 35 and 216, while the mean was approximately 60. Since the scales of the coefficients are quite different, we presented them in separate plots.

Statistics for calibration coefficients normal GRB sample



Statistics for calibration coefficients faulty GRB sample

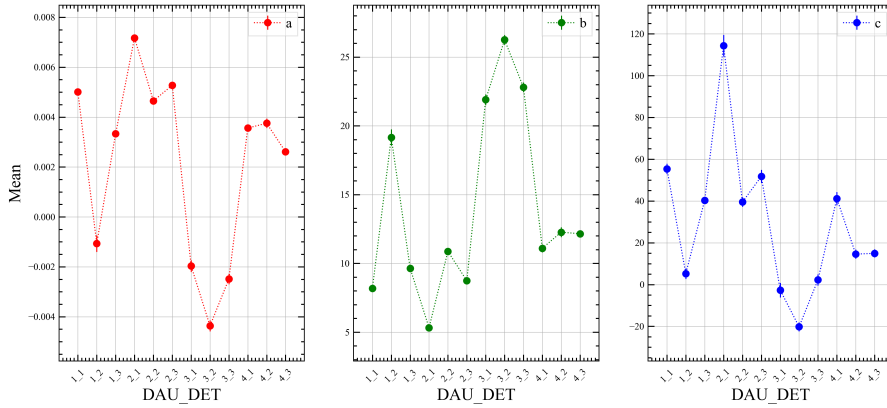


Figure 8: Top plot showing the calibration coefficients for all 12 detectors in the "good" GRBs, and the bottom showing it for the "bad" GRBs

5 Results and discussions

5.1 ASIM GRB database

5.1.1 GRB detections



Table 1 displays the index, GRB identification, classification type, ASIM trigger time, and corresponding coordinate information (right ascension, declination (J2000), magnetic latitude, and the incoming radiation angle on board ISS ϑ and φ) for the identified GRBs. There are 12 entries in the table, where each entry represents a GRB that has been detected simultaneously by either KW and/or FERMI.

Index	GRB	Type	T0	ra°	dec°	mlat°	ϑ°	φ°
1	180720B	L	2018-07-20 14:21:47.389	0.528	-2.917	38.5434	141.258	-42.464
2	181222B	S	2018-12-22 20:11:36.602	312.572	24.24	55.2793	100.622	-49.011
3	190206A	S	2019-02-06 03:49:28.525	313.33	-30.51	-54.2321	110.882	-36.976
4	190305A	S	2019-03-05 13:05:20.292	11.627	50.349	29.9766	133.903	-2.076
5	190606A	S	2019-06-06 01:55:06.782	76.561	-0.638	-47.4887	120.114	-20.997
6	200415A	S	2020-04-15 08:48:05.557	11.885	-25.263	-45.2905	70.643	-81.754
7	200521A	S	2020-05-21 12:16:39.004	169.531	7.222	-15.8446	130.710	-45.648
8	200716C	S	2020-07-16 22:57:40.634	196.01	29.644	39.4085	143.834	-140.018
9	201227A	S	2020-12-27 15:14:06.853	170.121	-73.613	14.4085	77.318	-50.463
10	210424B	S	2021-04-24 08:01:55.095	284.716	16.172	-32.3326	96.097	-17.705
11	210619B	L	2021-06-19 23:59:24.326	319.716	33.850	41.2906	135.591	-138.783
12	211211A	L	2021-12-11 13:10:03.113	212.271	27.884	46.4225	112.781	-177.757

Table 1: Table showing the index, GRB identification, classification type, ASIM trigger time, and corresponding coordinate information (right ascension, declination (J2000), magnetic latitude, and the incoming radiation angle on board ISS ϑ and φ) for the identified GRBs



5.1.2 GRB data availability

Table 2 presents the availability of data for each of the identified GRBs. The table shows whether the data is available for each of the instruments used in the analysis, namely LED, HED, KW, and FERMI. A "✓" indicates that the data is available, "x" indicates that the data is not available, and "-" indicates that the data exists but is not applicable. We can observe that for the majority of the GRBs, data is available from KW and/or FERMI. For this joint spectral analysis the LED-data have not been used, only HED-data.



GRB	LED	HED	KW	FERMI
180720B	-	-	-	-
181222B	x	✓	✓	✓
190206A	x	✓	✓	x
190305A	x	✓	✓	x
190606A	x	✓	✓	✓
200415A	-	-	-	x
200521A	x	✓	✓	x
200716C	x	-	✓	✓
201227A	x	✓	✓	✓
210424B	-	-	-	x
210619B	x	✓	✓	✓
211211A	x	✓	x	✓

Table 2: Data availability for LED, HED, KW, and FERMI. ✓ indicates that the data is available, x indicates that the data is not available, and - indicates that the data exists but is not applicable

5.1.3 GRB spectral intervals and ToF

GRB	Interval	KW		ToF	
		t_i	t_f	KW \rightarrow ISS	ISS \rightarrow GBM
180720B	—	—	—	-4.2377	-0.0051
181222B	1	0.0	0.512	2.8716	0.0026
—	2	0.128	0.256	—	—
190206A	1	0.0	0.064	4.9225	0.0189
190305A	1	0.768	1.280	3.4460	—
190606A	1	0.0	0.064	4.0316	-0.0081
200415A	1	—	—	4.1840	-0.0246
200521A	1	0.0	0.256	-0.6226	—
200716C	1	0.0	0.256	3.0155	0.0109
201227A	1	0.0	0.064	0.7142	-0.0008
210424B	1	—	—	-0.5033	0.0254
210619B	1	0.512	0.768	-2.6183	0.0227
—	2	0.0	2.048	—	—
211211A ¹	1	—	—	—	0.0049

Table 3: Spectral intervals used in the analysis and time of flight between instruments. All start and stop times are given relative to the KW T0 in seconds.

¹KW data not available. Spectrum $t_i = 5.9s$ and $t_f = 6.5s$ for HED and GBM



5.1.4 Model parameters

GRB	Int.	α	β	E_{peak}	χ^2/dof	C_A	C_F
181222B	1	$-0.538^{+0.025}_{-0.028}$	$-3.077^{+0.094}_{-0.143}$	365^{+10}_{-9}	265/204 (1.30)	$0.850^{+0.055}_{-0.062}$	$1.13^{+0.030}_{-0.032}$
—	2	$-0.118^{+0.045}_{-0.043}$	$-4.145^{+0.292}_{-0.359}$	430^{+11}_{-11}	198/181 (1.06)	$0.854^{+0.050}_{-0.047}$	$1.12^{+0.045}_{-0.042}$
190206A	1	$-0.318^{+0.088}_{-0.085}$	$-3.392^{+0.299}_{-0.544}$	1083^{+138}_{-102}	56/42 (1.32)	$2.71^{+0.229}_{-0.230}$	NA
190305A	1	$-0.179^{+0.073}_{-0.063}$	$-3.015^{+0.126}_{-0.143}$	435^{+20}_{-22}	89/68 (1.29)	$0.349^{+0.027}_{-0.025}$	NA
190606A	1	$-1.02^{+0.042}_{-0.044}$	$-2.14^{+0.157}_{-0.253}$	1748^{+882}_{-589}	138/104 (1.33)	$1.18^{+0.163}_{-0.158}$	$0.975^{+0.089}_{-0.078}$
200521A	1	$-0.392^{+0.087}_{-0.083}$	$-2.20^{+0.089}_{-0.079}$	1411^{+156}_{-268}	47/45 (1.05)	$1.37^{+0.109}_{-0.098}$	NA
200716C	1	$-0.537^{+0.099}_{-0.089}$	$-2.83^{+0.300}_{-0.729}$	702^{+107}_{-90}	129/141 (0.91)	$1.11^{+0.172}_{-0.144}$	$0.985^{+0.079}_{-0.073}$
201227A*	1	$-0.199^{+0.083}_{-0.067}$	$-3.57^{+0.508}_{-0.896}$	948^{+52}_{-68}	72/68 (1.05)	$1.22^{+0.125}_{-0.115}$	$1.36^{+0.084}_{-0.078}$
210619B	1	$-0.510^{+0.114}_{-0.116}$	$-2.165^{+0.053}_{-0.055}$	581^{+63}_{-57}	248/206 (1.12)	$0.922^{+0.070}_{-0.057}$	$1.18^{+0.048}_{-0.046}$
—	2	$-0.733^{+0.047}_{-0.038}$	$-2.217^{+0.028}_{-0.027}$	543^{+24}_{-28}	325/222 (1.46)	$0.848^{+0.033}_{-0.027}$	$1.13^{+0.03}_{-0.03}$
211211A	1	$-1.156^{+0.026}_{-0.018}$	$-2.68^{+0.108}_{-0.098}$	1368^{+68}_{-105}	194/152 (1.28)	$1.15^{+0.040}_{-0.038}$	1

Table 4: Model parameters in Xspec, using a normalization constant and the Band Model to validate the performance of ASIM against KW and FERMI. The focus is on ASIM (HED), C_A . The columns include GRB ID, spectral indices, peak energy, goodness of fit, and normalization constants. Errors given in 90% confidence range. For GRB201227A β is given in 1σ

One of the interesting parameters from this table is the normalization constant C_A , which measures the agreement between the HED and KW detectors. This parameter reflects how well the HED onboard ASIM performs in detecting high-energy events. A value close to unity means that the HED and KW detectors have similar counts, indicating a high performance of the HED. A value far from unity means that there is a discrepancy between the two detectors, indicating a low performance of the HED.

To verify that a higher value of the constant C_A indeed indicates an increase in counts, we utilized the astronomical event GRB 210619B as an example. By reducing the exposure time in the HED PHA file by half and fitting the data with the same model, we found that the value of C_A had doubled. This suggests that a larger value of C_A corresponds to an increase in the number of counts recorded, providing validation for this assumption.

It would be interesting to know how much the exposure should be reduced by in GRB181222B, GRB190206A and increased by in GRB190305A to get a normalization constant close to unity

Fried to modify the exposure for HED in GRB181222B. An increase in exposure from 0.512 s to 0.88 s produced a $C_A \sim 1$, but produced a bad fit with $\chi^2/\text{dof} > 2$

5.1.5 KW model parameters

GRB	Int.	Model	α	β	E_{peak} [keV]	χ^2 /dof
181222B	1	Band	$-0.520^{+0.085}_{-0.076}$	$-2.98^{+0.216}_{-0.314}$	368^{+28}_{-29}	52/61 (0.85)
—	2	Band	$-0.110^{+0.126}_{-0.112}$	$-3.53^{+0.410}_{-0.836}$	417^{+31}_{-32}	50/50 (1.00)
190206A	1	Band	$-0.501^{+0.101}_{-0.100}$	$-2.95^{+0.472}_{-2.95}$	1402^{+366}_{-324}	30/27 (1.11)
—	1	CPL	$0.567^{+0.091}_{-0.092}$	—	1593^{+252}_{-595}	31/28 (1.12)
190305A	1	Band	$-0.162^{+0.072}_{-0.067}$	$-2.96^{+0.127}_{-0.158}$	425^{+21}_{-21}	89/64 (1.40)
190606A	1	Band	$-0.645^{+0.515}_{-0.367}$	$-1.71^{+0.150}_{-0.218}$	435^{+308}_{-202}	22/21 (1.05)
200521A	1	CPL	$0.259^{+0.131}_{-0.141}$	—	1333^{+195}_{-166}	34/43 (0.79)
200716C	1	Band	$-0.544^{+0.208}_{-0.163}$	$-2.31^{+0.284}_{-0.620}$	667^{+180}_{-153}	54/48 (1.13)
201227A	1	CPL	$0.19^{+0.370}_{-0.003}$	—	882^{+138}_{-114}	21/22 (0.95)
210619B	1	Band	$-0.427^{+0.122}_{-0.109}$	$-2.06^{+0.090}_{-0.114}$	587^{+94}_{-78}	92/74 (1.24)
—	2	Band	$-0.500^{+0.061}_{-0.057}$	$-2.01^{+0.036}_{-0.039}$	433^{+30}_{-28}	145/93 (1.56)

Table 5: Model parameters from all the available KW spectrums. Some are fitted with the Band model, while others are fitted with the cutoff powerlaw model

5.1.6 Normalization constant



Anomalies found for a set of GRB's. Discuss the cause for this deviation (background rate, exposure time, wrong spectrum accumulation, occultation by modules onboard ISS, etc

5.1.7 Correlation between KW-ASIM and KW spectral analysis

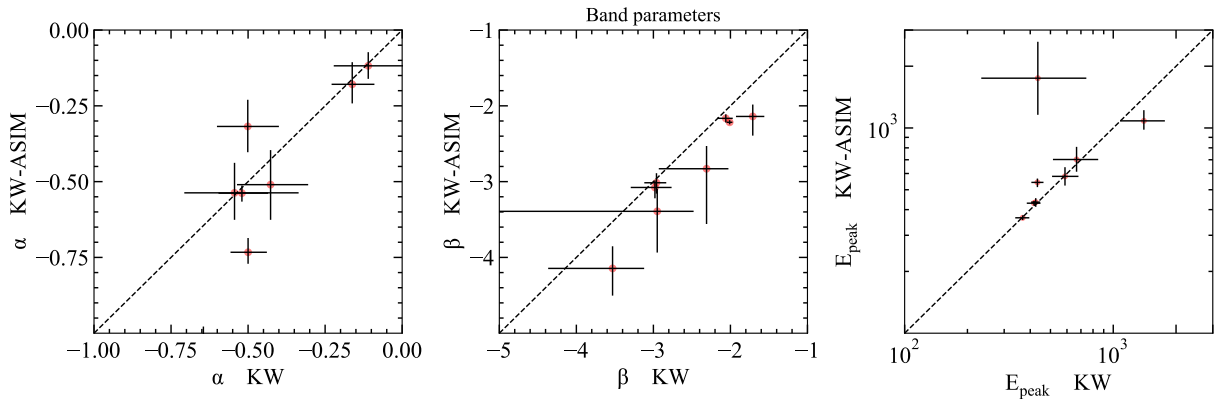


Figure 9: Scatter plots showing the correlation between the Band parameters α , β , and E_P obtained for the KW-ASIM and KW-only spectral analysis. The horizontal and vertical lines indicate the upper and lower error bars. A dashed black line is plotted in each subplot, indicating the line of equality where the values from both models would be the same.

Figure 9 presents three scatter plots that depict the correlation between the Band parameters α , β , and E_{peak} obtained for the KW-ASIM and KW-only spectral analysis. Each subplot displays the values of one parameter obtained from the KW-only model on the x -axis and the corresponding values obtained from the KW-ASIM model on the y -axis. The horizontal and vertical lines represent the upper and lower error bars. Additionally, a dashed black line is plotted in each subplot to indicate the line of equality where the values from both models would be the same. Note that the KW data have been cleaned from the CPL model parameters found in Table 5. However, it is essential to keep in mind that the spectral analysis of the KW data only for some bursts is best fitted by a CPL model, not the Band model.

Although KW-ASIM values are generally consistent with KW-only values, some deviations from the line of equality are observed, particularly for the E_P plot. In this case, the KW-only value is significantly less than the corresponding KW-ASIM value, and the outlier is GRB190606A. The discrepancy is due to the energy band on which the data is fitted, as HED has a higher energy band, and the joint fit was performed up to 40 MeV. Therefore, it is expected that the E_P will be significantly higher since this is a hard burst. Furthermore, it is worth mentioning that the reported E_P -value in the GCN for the KW spectrum of this particular burst is 664(+1038, -388) keV.

In the β -plot, we observe that the KW-only parameters are generally less than the corresponding KW-ASIM values, and one outlier is worth mentioning in this particular plot, which is GRB190206A. This burst has a large negative horizontal error because the KW-only spectrum is fitted with a Band model when the obvious better choice is the CPL model. Please refer to Table 5 for exact values.

5.1.8 Calibration Coefficients for KW-ASIM-FERMI and KW-ASIM Spectral Analysis

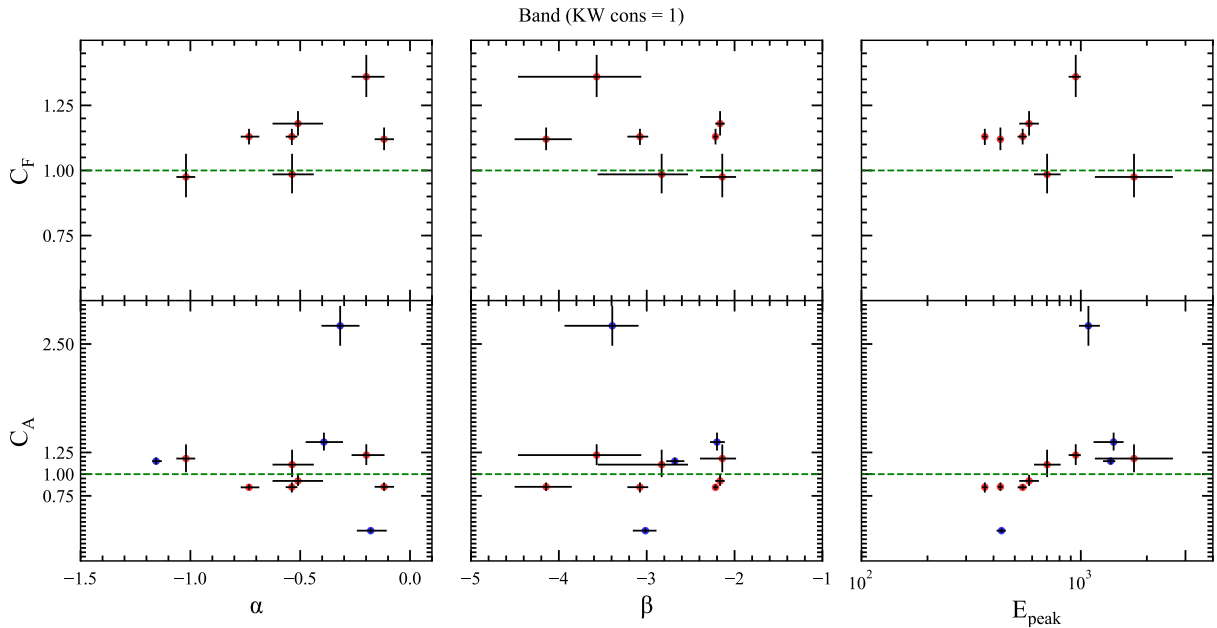



Figure 10: This stacked scatter plot shows calibration coefficients obtained for KW-ASIM-FERMI and KW-ASIM joint spectral analysis using *xspec*. The top three subplots display C_F as a function of α , β , and E_{peak} for KW-ASIM-FERMI joint spectral analysis, while the bottom three subplots display C_A for KW-ASIM joint spectral analysis. Red dots represent KW-ASIM-FERMI joint spectral analysis data, and blue data points represent KW-ASIM joint spectral analysis data. The green dashed line in each subplot shows the expected calibration coefficient of unity. Each subplot shows upper and lower error bars, and there are additional data points from four bursts in the bottom row of each subplot.

In figure 10 we see a stacked scatter plot displaying the calibration coefficients obtained for the KW-ASIM-FERMI and KW-ASIM joint spectral analysis. As mentioned in earlier section (5.1.4), the calibration coefficients C_F and C_A were obtained through joint spectral analysis using *xspec*. The figure shows six subplots, with the top three displaying the calibration coefficients C_F as a function of the spectral parameters α , β , and E_{peak} for the KW-ASIM-FERMI joint spectral analysis. The bottom three subplots display the calibration coefficients C_A as a function of the same spectral parameters, but for the KW-ASIM joint spectral analysis. The red dots in each subplot represent the calibration coefficients obtained from the KW-ASIM-FERMI joint spectral analysis, while the blue data points represent the KW-ASIM

joint spectral analysis. The vertical and horizontal lines show the upper and lower error bars. The green dashed line in each subplot represents the optimal calibration coefficient value of 1. There are four additional data points in each subplot in the bottom row for the KW-ASIM joint spectral analysis; these are data points from GRB190206A, 190305A, 200521A and 211211A. In these additional data points we observe two large deviation of C_A from unity. These are caused by the bursts GRB190206A and GRB190305A. 

5.2 Case studies

General introduction to our case studies. What new information have these given us? What was my role in these case studies? What have Maria talked about in her papers?

5.2.1 GRB 210619B

5.2.2 GRB 211211A

Interesting burst, GW detection, merger of compact objects (possible NS-BH), kilonova (1e3 more luminous than regular supernova, hence the name)

5.3 GRB classifications

5.4 ASIM performance assessment and outlook

6 Summary and outlook

7 Appendix I: GRB Archive

8 Appendix II: ASIM Fits Software

9 Appendix III: Code & Data

10 Abbreviations

References

- [Bachetti et al., 2022] Bachetti, M., Huppenkothen, D., Khan, U., Mishra, H., Sharma, S., Stevens, A., Swinbank, J., Desai, A., Rashid, H., Ribeiro, E. M., Tripathi, M., Sipőcz, B., Vats, D., tappina, omargamal8, Davis, M., Rasquinha, A., Balm, P., Mumford, S., Campana, R., parkma99, Garg, N., Tandon, A., Hota, A., Nick, Raj, R., Mishra, S., Smith, A., Mahlke, M., and Sachidanand, S. (2022). Stingraysoftware/stingray: v1.1.
- [Lindanger et al., 2021] Lindanger, A., Marisaldi, M., Sarria, D., Østgaard, N., Lehtinen, N., Skeie, C., Mezentzev, A., Kochkin, P., Ullaland, K., Yang, S., et al. (2021). Spectral analysis of individual terrestrial gamma-ray flashes detected by asim. *Journal of Geophysical Research: Atmospheres*, 126(23):e2021JD035347.